J Nanostruct 9(2): 287-300, Spring 2019

RESEARCH PAPER

Experimental Study of Methylene Blue Adsorption from Aqueous Solutions onto Fe_3O_4/NiO Nano Mixed Oxides Prepared by Ultrasonic Assisted Co-precipitation

Gheffar Kheraldeen Kara, Mahboubeh Rabbani*

Department of Chemistry, Iran University of Science and Technology, Tehran, Iran

ARTICLE INFO

Article History:
Received 04 January 2019
Accepted 08 March 2019
Published 01 April 2019

Keywords:
Adsorbent Dose
Methylene Blue
Mixed Metal Oxide
Novel Adsorbent

ABSTRACT

According to the increasing development of the mankind, social and technology activities in the earth, various industry is in a state of uncontrolled growth. In the present study, magnetite/nickel oxide mixed metal oxide nanoparticles (FNMMO NPs) were prepared by a simple method assisted by ultrasonic waves and applied as a novel adsorbent to dispose of dye wastewater. The morphology and chemical structures of the Fe_3O_4, NiO and FNMMO NPs were characterization by Fourier transform infrared (FT-IR), X-ray diffraction (XRD), vibrating sample magnetometer (VSM), energy-dispersive X-ray spectroscopy (EDX), scanning electronic microscope (SEM) and transmission electron microscope (TEM). The adsorption of methylene blue (MB) onto FNMMO NPs was studied in relation to initial concentration of MB, contact time, adsorbent dose and pH value of solution. The equilibrium adsorption isotherm was fitted by Langmuir isotherm. The capacity of adsorption was evaluated 40.1 $mg.g^{-1}$ and the time required to reach the adsorption equilibrium was 180 min.

How to cite this article
Kheraldeen Kara G, Rabbani M. Experimental Study of Methylene Blue Adsorption from Aqueous Solutions onto Fe_3O_4/NiO Nano Mixed Oxides Prepared by Ultrasonic Assisted Co-precipitation. J Nanostruct, 2019; 9(2): 287-300. DOI: 10.22052/JNS.2019.02.011

INTRODUCTION

According to the increasing development of mankind, social, and industrial activities in the earth cause the contamination of water, which is a current problem all over the world and in the state of this uncontrolled growth [1,2]. The wastewater of the textile industries is known to contain a considerable large amount of non-fixed dyes, azo dyes and inorganic salts that exclusion them from waters is beneficial [3,4]. Methylene blue (MB) is widely used in cotton, wools and silks dyeing. Acute exposure to MB will cause a series of physiological responses such as heart rate increasing, vomit and peril disease like dyspnea, tachycardia, cyanosis, etc. [5-7]. Therefore, elimination it from wastewater has attracted considerable attention. Many methods such as biological method [8], chemical oxidation method [9], adsorption method [10], etc, have been applied for removal of organic dyes from wastewater.

The mixed metal oxides play an important key in wide techniques like photocatalysts, manufacture of a hard parts and absorbents, because exhibit some specific properties of them [11-14]. Using two methods at the same time to produce nano-structure materials in preparation of catalysts has greatly influenced the physical and chemical virtues of these materials. The main advantages of these mixed methods include increasing efficiency, reducing energy and raw materials consumption, augmenting the activity and stability of the catalyst, enhancing selectivity and its surface, etc [15]. In the last decade, valuable scientific approaches to beget nano materials have been performed on

* *Corresponding Author Email: m_rabani@iust.ac.ir*

numerous classes of ultrasonic, because ultrasonic irradiation can generate microbubbles in liquid, the cavitational collapses of which procreate exceedingly high temperature (~5000 K), pressure (~1000 atm), high heating and cooling rates (>9-10 K/sec), etc [16]. Previous studies indicated that such extreme chemical and physical environment was helpful to increase the rate synthetic reactions and to obtain smaller crystals with more uniform size distribution compared to conventional techniques for synthesizing the nanoscale materials [17,18]. Recently, Arani et al [19] reported that iron vanadate-sphere like particle was sonochemically synthesized in aqueous phase. Maleki et al [20], reported that by ultrasonic waves Fe_3O_4@clay was synthesized. Valencia et al [21] used ultra-irradiation to synthesis Fe_3O_4@ Ti_xO_y/activated carbon. Dan Li et al [22] heirachical core/shell ZnO/NiO had been prepared via a simple ultrasonic spray pyrolysis process. Yudin et al [23] reported that NiO hollow nanostructure powder were synthesized by ultrasonic spray pyrolysis technique. Nanocomposite NiO/Ag_3VO_4 was prepared by ultrasonic assisted preparation to study the photocatalytic activity [24].

Recently, among all the magnetic nanomaterials, Fe_3O_4 (magnetite) is the important material due to its applications in wide areas such as biomedical ,tumor ,physiocochemical properties and target drug delivery. Magnetic virtues nanosized systems such as bulk-like and their preparation and have been active research topics in material science [25-27]. Nickel oxide)NiO(has attracted much important field for example in catalysis, as an electrode material and sensors. These days the focus is on building on new and various of nanostructures, and possesses a variety of distinctive properties. Corre-shell serve as new combination at the nanoscale, this is modern mixture contains interesting advantage, for example, magnetic properties of the core and optical properties of the shell, which was observed in the case of "Au" nanoparticles [28,29].

In the present paper, the magnetite/nickel oxide mixed metal oxide nanoparticles (FNMMO NPs) with a good compatibility was synthesized in a one-step co-precipitation assisted by ultrasonic irradiation in which alkaline solution was synchronously added drop-wise into an aqueous phase with the aid of ultrasound. This FNMMO NPs has a good benefits such as: low-toxicity and magnetic property, as environmental friendly metal mixed oxides, used an appropriate adsorbent of MB for the first time, the method preparation is economic and doesn't need to harmful solvent. The size, structure and magnetic properties of the mixed metal oxides were characterized using different analytical tools. The adsorption capability was demonstrated using methylene blue (MB) as the model compound because of their extensive

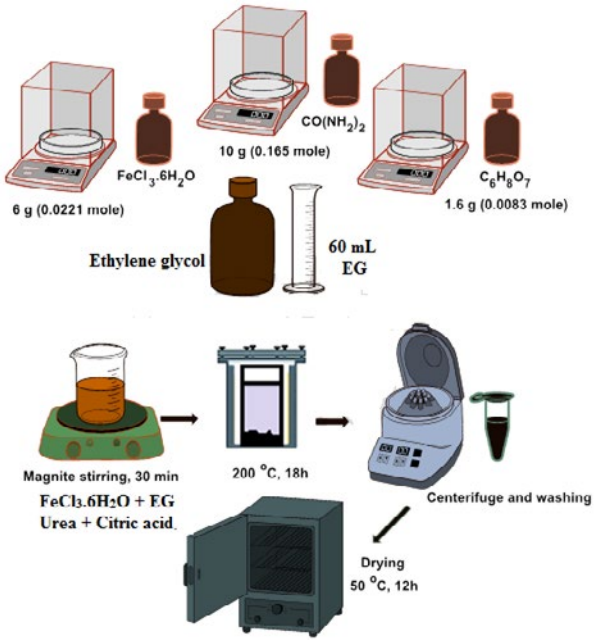

Scheme 1. The synthesis processor of Fe_3O_4 NPs via solvothermal method.

use in various industries. Methylene blue is a cationic dye which is toxic and carcinogenic. The adsorption behaviors of Fe_3O_4/NiO towards MB adsorption were studied using equilibrium viewpoint. The effects of several parameters such as pH, initial MB concentration, adsorbent dosage and contact time were investigated in this report.

MATERIALS AND METHODS

All the analytical chemicals were purchased from Merck Co. and used as-received without further purification. For preparing superparamagnetic Fe_3O_4 nanoparticles, NiO nanoparticles and Fe_3O_4/NiO nanoparticles, ferric chloride hexahydrate ($FeCl_3.6H_2O$), urea (CH_4N_2O), citric acid ($C_6H_8O_7$), absolute ethylene glycol (EG), ethanol, nickel acetate ($Ni(OAc)_2.4H_2O$) and sodium hydroxide (NaOH) were used.

Synthesis of Fe_3O_4 nanoparticles

Fe_3O_4 nanoparticles were synthesized through a solvothermal method [30]. 0.0221 mole $FeCl_3.6H_2O$ (6 g), 0.165 mole urea (10 g) and 0.0083 mole citric acid (1.6 g) were loaded into a 100 mL Teflon-lined stainless steel autoclave, which was then filled 60 mL absolute EG heated to 200 °C and maintained there for about 18 h. After cooling to room temperature naturally, the black products were filtered off, washed with distilled water and ethanol for several times and dried in vacuum at 50 °C for 12 h. Scheme 1 shows the synthesis processor of Fe_3O_4.

Synthesis of Fe_3O_4/NiO nano mixed oxide

Fe_3O_4/NiO mixed oxide nanoparticles were synthesized with stoichiometric ratio (1:1) by ultrasonic assisted co-precipitation method (Scheme 2). In a typical experimental procedure, 0.0023 mole Fe_3O_4 (0.52 g) was re-dispersed in 30 mL deionized water by sonication before adding 0.0023 mole nickel acetate $Ni(OAc)_2.4H_2O$ (0.416 g) to it, the mixture was exposed to ultrasonic waves for 1 h at power 40 W/m^2 with a 5 min pulse and 2 min silent period cycle. Then sodium hydroxide aqueous solution (1 M) was added slowly under stirring up to pH around 12. The resulted black solution was transferred into a round-bottom flask and kept at 120 °C for 3h. After cooling to room temperature, the black product was collected by strong magnet, then dried at 60 °C for 7 h. Fe_3O_4/NiO was obtained via the calcination of the as-made $Ni(OH)_2$ at 500 °C for 2 h.

For comparison, pure NiO nanoparticles were synthesized by above mentioned process without

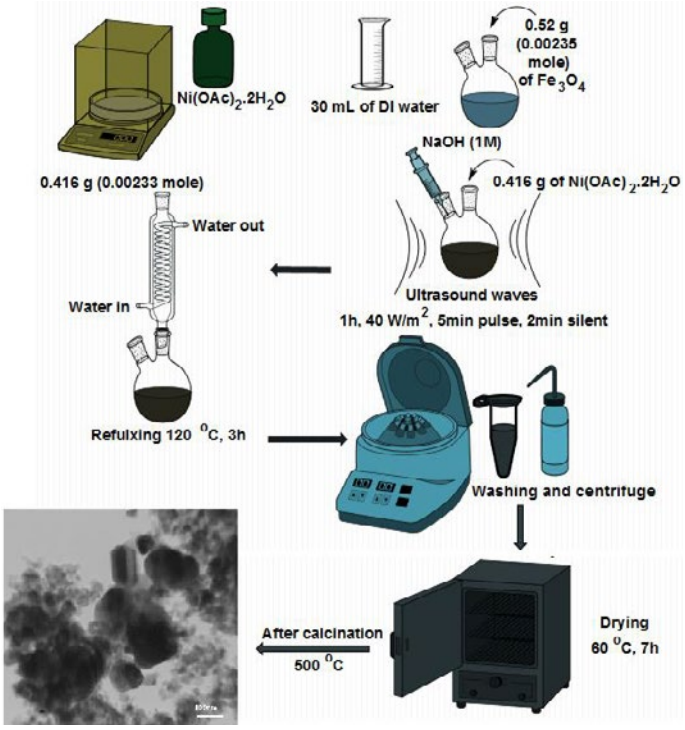

Scheme 2. The synthesis processor of Fe_3O_4/NiO via co-precipitation method assisted by ultrasonic.

adding of Fe_3O_4. The temperatures of calcination for preparation of NiO were 320 and 500 °C.

Characterization of nanoparticles

The as-prepared samples were characterized by a X-ray diffractometer (XRD, JEOL diffractometer with monochromatic Cu Kα radiation, λ=1.5418 Å), scanning electron microscope (SEM, AIS2100, Seron Technology) and transmission electron microscope (TEM, Philips, CM30). The FT-IR analyses were carried out on a Shimadzu FT-IR-8400 spectrophotometer using KBr pellet for sample preparation. Also a commercial HH-15 model vibrating sample magnetometer (VSM, Lake Shore 7410) was used at room temperature to characterize the magnetic properties of Fe_3O_4 and Fe_3O_4/NiO. Energy dispersive X-ray (EDX) was employed for elemental analysis of adsorbent using (SEM, AIS2100, Seron Technology).

Evaluation of adsorption activity

The adsorption of MB in aqueous solution on the as-prepared FNMMO NPs was performed in a batch experiment. 0.05 g of the FNMMO NPs as adsorbent was added into 50 mL of MB solutions of desired initial concentration 10 $mg.L^{-1}$ under shaker. At predetermined time intervals, the samples were removed from the solution by magnetic separation. The effect of pH on the adsorption of MB on the FNMMO NPs adsorbent was studied over pH range of 4-12. The pH was adjusted by adding aqueous solutions of 0.1M HCl or 0.1M NaOH. To determine the effect of adsorbent dosage on MB adsorption, experiments were conducted by varying the adsorbent dosage (0.025-0.15 g.10 mL^{-1}) in the sample solution for a fixed initial dye concentration of 10$mg.L^{-1}$. The effect of time contact on the adsorption of MB on the FNMMO NPs adsorbent was investigated in the range (30-180 min). The concentrations of dye were determined by using a Shimadzu UV-vis. spectrophotometer at λ_{max} =664 nm. The amount of MB adsorbed per unit mass of the adsorbent was evaluated by using the mass balance equation as follows:

$$q = \frac{(C - C_e) * V}{m} \quad (1)$$

Where q ($mg.g^{-1}$) is the amount adsorbed per gram of adsorbent, C and C_e ($mg.L^{-1}$) are initial and equilibrium concentration of MB in the solution, respectively, m (g) is the mass of the adsorbent used, and V (L) is the initial volume of the MB solution.

The percentage of removal efficiency (X %) is given by:

$$S = \frac{A - A_0}{A} * 100 \quad (2)$$

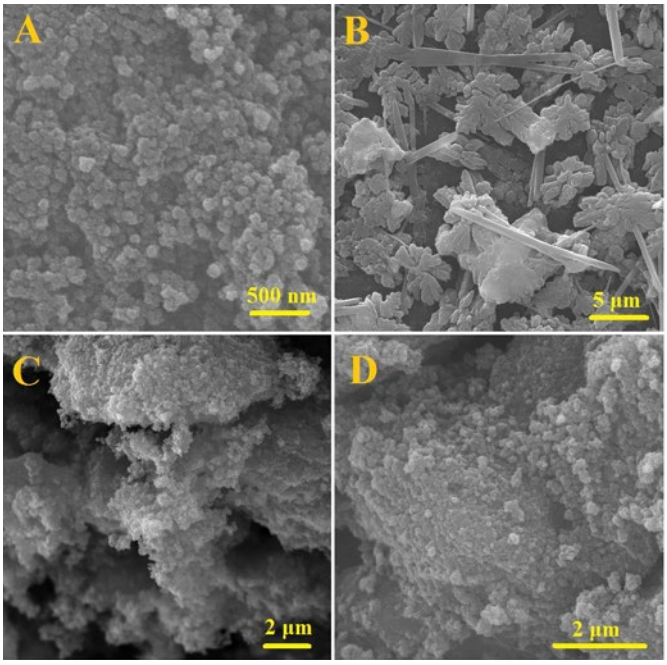

Fig. 1. SEM images of (A) Fe_3O_4 NPs, (B) NiO NPs calcined at 320 ºC, (C) NiO NPs calcined at 500 ºC and (D) Fe_3O_4/NiO nano mixed oxide calcined at 500 ºC.

Where A_0 and A are the concentration of dye at times of 0 and t, respectively.

All batch experiments were carried out at ambient temperature (25 ± 2 °C) and all the suspensions were shaken on the rotary shaker at 300 rpm for 3 h.

RESULTS AND DISCUSSION

Characterization

Morphology study

The morphologies of all synthesized structures as adsorbent were obtained by SEM technique shown in Fig. 1. For Fe_3O_4 (Fig. 1(A)), the presented particles are shown similar shape and sizes in the range of 60-75 nm. These particles are well uniformly and agglomerated, that show with a rough surface. Fig. 1(B) illustrates the SEM image of micro-NiO, which calcined at 320 °C, these structures are explained microcaliflower with the microstructure of sword. Fig. 1(C) shows the SEM image of agglomerated NiO nanoparticles prepared at 500 °C. These particles are with diameter in the range 100-200 nm. Fig. 1(D) shows the SEM image of FNMMO NPs that was prepared at 500 °C. It was observed that the Fe_3O_4 were successfully modified by NiO to form small sizes of FNMMO NPs. These samples have diameter in the range of 60-70 nm. Fig. 2 exhibits the TEM images of FNMMO having small sphere-like morphologies in general, and the diameter of those are ranging between 60-100 nm. The above results indicated that the FNMMO NPs have been successfully synthesized.

XRD patterns of samples

The XRD pattern of the Fe_3O_4, NiO, and FNMMO NPs was presented in Fig. 3. It shows that the diffraction peaks correspond to the (1 0 1), (2 2 0), (3 1 1), (4 0 0), (4 2 2), (5 1 1) and (4 4 0) suggests the particles could be easily indexed to Fe_3O_4, which can be observed at 2Θ = 28.81, 30.1, 35.53, 43.11, 56.68, 57.09 and 62.8°, respectively. All of the identified peaks in the XRD pattern can be attributed to magnetite Fe_3O_4, based on the standard data for magnetite (JCPDS Card, No. 01-075-1609). The XRD pattern of pure NiO exhibited main peaks at 2Θ = 36.52, 43.38, and 62.3°, which can be ascribed to the (1 1 1), (2 0 0) and (2 2 0) planes, respectively. All of the identified peaks in the XRD patterns can be attributed to NiO based on the standard data for NiO (JCPDS Card, No. 01-075-0197). In the XRD pattern of FNMMO NPs, there were six major reflections that appeared in Fig. 3(A) located at about 2Θ = 30.1, 35.52,

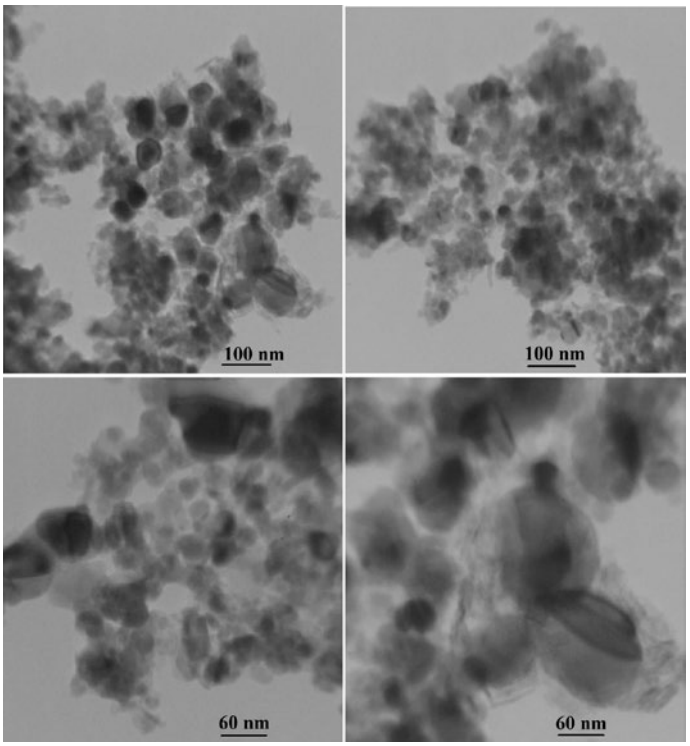

Fig. 2. TEM images of FNMMO calcined at 500 ºC.

43.3, 56.6, 57.09 and 63,3°, respectively, that are in good agreement with them. According to the Debye-Scherrer equation, as shows in shown in equation:

$$d = \frac{k * \lambda}{\beta * \cos\theta} \quad (3)$$

where the constant k is 0.94, β is the full width of the peak at half maximum high (FWHM), λ is the wave length of Cu-Kα radiation of the X-ray source 1.5405 Å, and d is the diameter of the crystallite. The peak at 2Θ= 35.5, 43.38, and 63.5° was used to estimate particles size that calculated values obtained 40.7, 25.7, 65.2 nm.

FT-IR spectra of samples

FT-IR spectra of prepared pure Fe_3O_4, pure NiO and Fe_3O_4/NiO nano mixed oxide in the range 400-4000 cm^{-1} were indicated in Fig. 4. In the spectra of Fe_3O_4, the strong and the sharp absorption band appeared at 570 cm^{-1} is the good agreement with vibration band of Fe-O as typical band of reverse spinel iron oxide. Absorption peak at 3490 cm^{-1} associated to O-H vibration. The other peaks were observed at 1039-3444 cm^{-1} that related to C-O, C=O, N-C-N and C-H bonding on citric acid and urea have not been completely removed from Fe_3O_4 NPs synthesized by solvothermal method. The FT-IR spectra of NiO shows the strong and the sharp adsorption band appeared at 495 cm^{-1} in good agreement with vibration band Ni-O as the typical band of nickel oxide. In the spectra of Fe_3O_4/NiO, the sharp absorption band appeared at 568 cm^{-1} is in the good agreement with merged vibration bands of Fe-O and Ni-O as typical band of mixture oxide. The peak observed at 1041 cm^{-1} can be related to C-O bonding of acetate salt. The peak at 2390 cm^{-1} belongs to C-H bonding of acetate

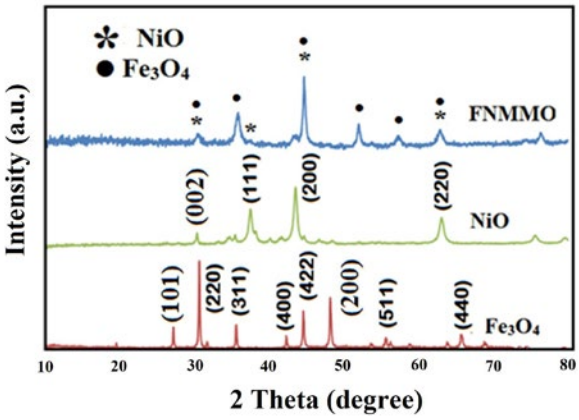

Fig. 3. XRD plots of Fe_3O_4, NiO and Fe_3O_4/NiO.

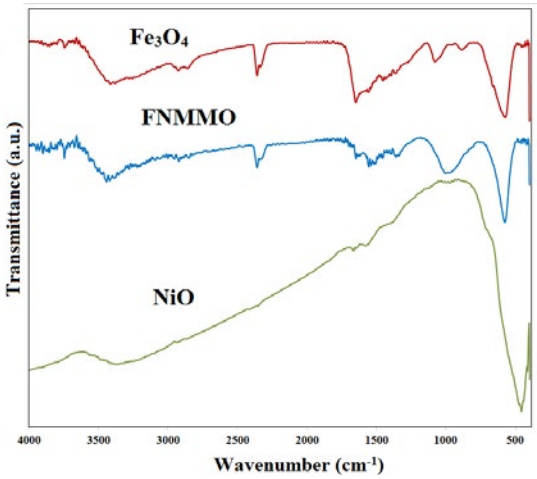

Fig. 4. FT-IR spectra for Fe_3O_4, NiO and FNMMO.

salt. These peaks observed that acetate salt have not been completely removed from Fe_3O_4/NiO nano mixed oxide synthesized by co-precipitation method.

VSM analysis of samples

Fig. 5 shows the magnetic hysteresis loop of Fe_3O_4 and FNMMO NPs. The saturation magnetization value (Ms) of Fe_3O_4 NPs and FNMMO NPs was measured to be 53.44 and 35.60 emu/g, respectively. It should be noted that almost no hysteresis loops were found in the magnetization curve, suggesting the superparamagnetice of Fe_3O_4 and FNMMO NPs. As seen in this figure, it known that the curve of FNMMO NPs exhibits lower saturation magnetization than curve of pure Fe_3O_4. Magnetic properties of materials are general influenced by many factors such as size of particles, structure, surface disorder and morphology [31]. Therefore, lower Ms of FNMMO NPs can be due to high temperature calcination up to 500 °C for NiO.

EDX analysis

The EDX analysis of FNMMO are represented in Fig. 6. This analysis revealed high elemental of oxygen (~>85 %) rather than metal content of FNMMO NPs. Attention to the EDX analysis, it is

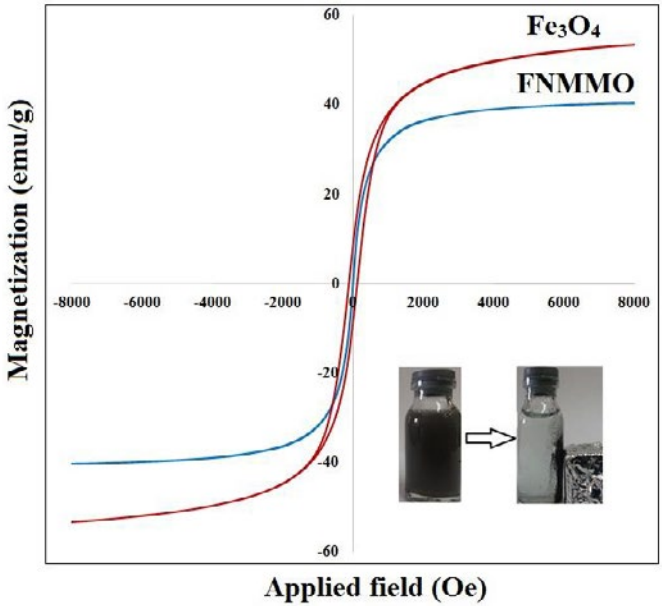

Fig. 5. The magnetic properties of pure Fe_3O_4 and FNMMO.

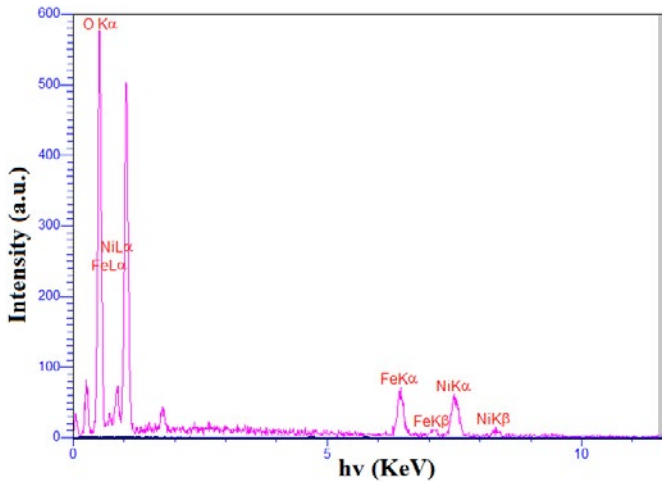

Fig. 6. EDX spectra of FNMMO NPs.

noted that the Fe/Ni ratio is equal, this proves the accuracy of the experimental work in which the FNMMO NPs was prepared by 1:1 molar ratio.

Analysis of FNMMO NPs after MB adsorption

The XRD, FT-IR and EDX studies of FNMMO NPs before and after MB adsorption on their surface

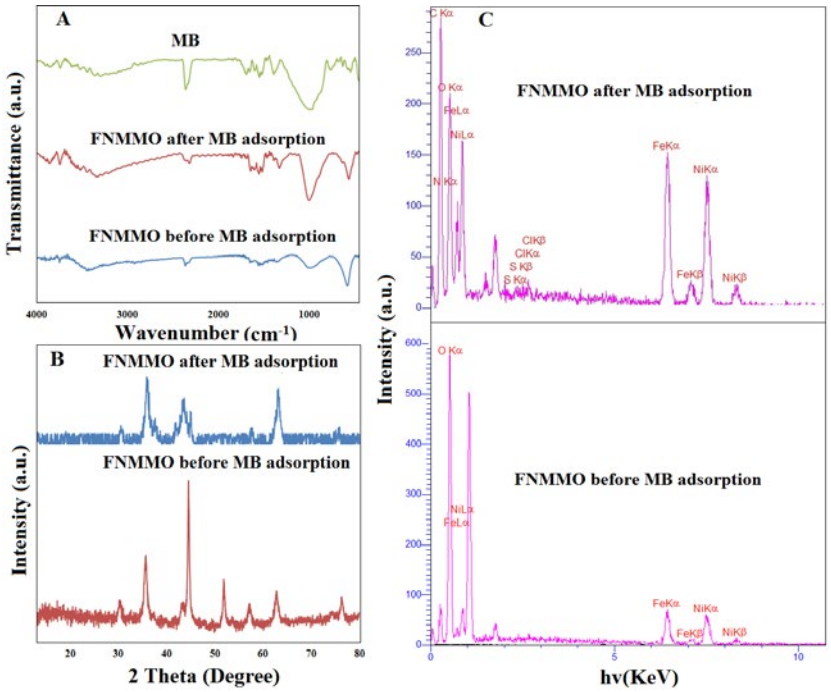

Fig. 7. (A) FT-IR spectra, (B) XRD patterns and (C) EDX analysis of FNMMO before and after MB adsorption.

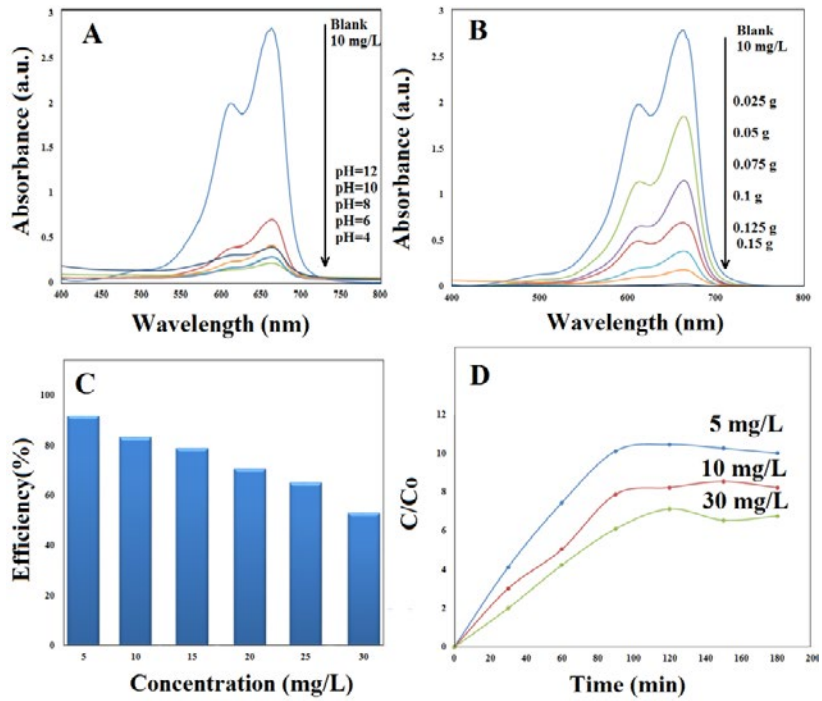

Fig. 8. (A) Study of MB adsorption onto Fe_3O_4/NiO at various of pH, (B) adsorption of MB onto Fe_3O_4/NiO in presence of various weight of adsorbent, (C) removal efficiency of MB onto Fe_3O_4/NiO at different concentrtiaon of dye and (D) Study of MB adsorption onto Fe_3O_4/NiO at various time.

are necessary to show the chemical composition and stability of the adsorbent in this processes. The FT-IR spectra of FNMMO after MB adsorption (Fig. 7(A)) shows strong signature of MB indicating the adsorption of MB on the surface of FNMMO NPs. The FT-IR spectrum of FNMMO NPs without adsorbed dye molecules and pure MB is shown for comparison. Several function group peaks were detected on FNMMO NPs after adsorption. The active functional groups on the FNMMO NPs that participated in binding the MB molecules were 1326, 1315, 1645-1514, 3280, 3211 3444-3344, 3863-3745, 1100-1300 and 3860-3740 cm^{-1} representing the C=C (that is in aromatic rings), C-N symmetrice, C-C, -CH_3, C-H aromatic, -OH, C-S and –N-H groups, respectively.

The XRD pattern of the FNMMO NPs after MB adsorption presented in Fig .7(B) indicated that crystallinity structure of FNMMO NPs have been remained after adsorption processing. Although, the intensity of some peaks have been changed. This suggests that the MB adsorb mostly by physicsorption, as a result of the adsorption reaction.

The chemical composition of the composite after adsorption was demonstrated by EDX spectra (Fig .7(C)). The presence of C, S, N and Cl indicates that FNMMO NPs have well adsorbed MB molecules.

Study of adsorption activity

The effect of pH

The pH value, which can control the protonation of the functional groups, is an important factor for adsorption process. The adsorption experiments were carried out by varying pH range from 4 to 12, and the results are illustrated in Fig. 8(A).

The pH is one of the main factors influencing on the adsorption rate of some organic compounds in the adsorption processes. It is an important operational variable in actual wastewater treatment, too. The adsorption of MB at different pH (4, 6, 7, 8, 10 and 12) was shown in Fig. 8(A) clearly revealed that the best result was obtained in acidic solution (pH=4, X%= 92%). The surface charge of Fe_3O_4/NiO is presumably positively charged by H^+ in acidic solution and negative by OH^- charged in alkaline solution. MB has chloride group (Cl^-) which is negative charged, therefore the acidic solution favors adsorption of dye onto adsorbent surface, thus the adsorption efficiency increases. The adsorption of MB in alkaline solutions is probably low due to the formation of group OH^- as it can be rebated with pollutant surface.

The effect of FNMMO dosage

From an economic point of view, the study of adsorbent mass is useful for selecting the appropriate amount of adsorbent for industrial applications. The effect of adsorbent dose on the percentage uptake of MB was studied pH=4, and 25 °C with 50 mL of 10 $mg.L^{-1}$ dye solution with varied amount of FNMMO NPs (0.025-0.15 g). Fig. 8(B) shows the effect of adsorbent dose on uptake capacity. Percentage adsorption was found to increase from 32.71% a dose of 0.025 $g.L^{-1}$ to 98.92% a dose of 0.15 $g.L^{-1}$. Increase in the percentage adsorption may be due to the increase of the number of active sites on surface with the increasing amount of adsorbent dose [32].

Effect of dye concentration

The initial concentration of the MB dye solution has a significant effect on color removal. It can be seen from Fig. 8(C) that the color removal of MB solution onto FNMMO NPs by adsorption

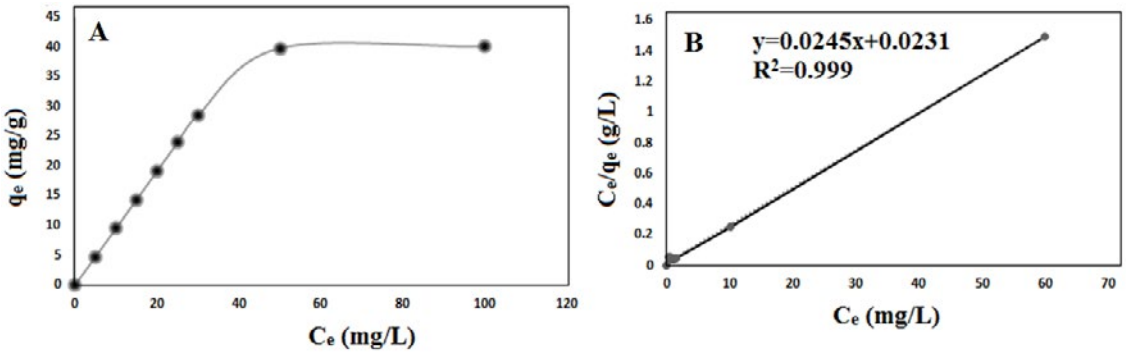

Fig. 9. (A) Adsorption isotherm of MB on Fe_3O_4/NiO (conditions: ambient temperature, pH=4 and 0.05 g of Fe_3O_4/NiO as adsorbent) and (B) Langmuir plots for the adsorption of MB.

rose rapidly at the beginning, which efficiency of removal was measured (X=92%), then gradually slowed down until equilibrium was reached. It might be explained that the large number of vacant surface sites were available for adsorption during the initial stage. For the concentration of 20, 25 and 30 mg.L^{-1}, MB removal reached at about 62%, 58%, and 45% in 3 h, respectively. Around 92% and 82% adsorption was observed for initial concentration of 5 and 10mg.L^{-1} within 3h. The results can be attributed to an increase in the driving force of concentration[15].

Effect of adsorption time

The influence of contact time on the adsorption time capacity of Fe_3O_4/NiO is depicted in Fig. 8(D) for MB solutions with concentrations of 5, 10 and 30 mg/L. The adsorption of MB onto Fe_3O_4/NiO was investigated at different time (30, 60, 90, 120, 150 and 180 min) at pH=4 which clearly are explained that the best results were reaped a good ability to remove of MB at 180 min from aqueous solutions. |However, Fe_3O_4/NiO nano mixed oxide show a greater ability, (approximately X%=92%, 89% and 81% for 5, 10 and 30 mg/L adsorption, respectively) after 180 min contact time. This can be explained by the additional adsorbing sites that provided by the oxygen atoms of iron oxide nanoparticles, on the surface of mixed oxide which are also available for electrostatice interaction with Fe_3O_4/NiO. It should be noticed that in the composite there are two sorts of adsorbing sites, iron oxide and nickel oxide nanoparticles [33].

Adsorption isotherm

The capacities of Fe_3O_4/NiO nano mixed oxide to adsorb MB were investigated by measuring the intial and final concentration of MB in adjusted pH=4. Fig. 9(A) shows that the adsorption of MB dye increases with increase in dye concentration and inclines to achivieve saturation point at higher concentration. The Langmuire equation, a well know adsorption isothermal model, was used to analyze the relationship between the amount of MB adsorbed onto Fe_3O_4/NiO and its equilibrium concentration in solution. Langmuir's model does not consider the vibriation in adsorption energy, but it clearly describes the adsorption procedure.

The general form of Langmiure isotherm equation is as follows:

$$\frac{q_e * a_l}{K_l} = \frac{K_l * C_e}{(1 + K_l * C_e)} \quad (4)$$

Where q_e is the amount of dye adsorbed per unit of adsorbent at equilibrium concentration of the MB in the solution (mg/L) and a_L (L/mg) and K_L (L/g) are the Langmiure constant. In addition, the maximum adsorption capacity (mg/g) is indicated by (Q_m=K_L/a_L). As the q_{max} depends on the number and structure of the adsorption sites, current study aimed at synthesizing Fe_3O_4/NiO nano mixded oxide to increase the number of avaialble sites. As long as there are unoccupied sites, adsorption process will increase with increasing MB concentrations, but as soon as all of the sites are occupied, a further increase in concentration of MB solutions does not the amount of MB on adsorbents. Equation below can be rearrangeed into a linear form: The values of (a_L) and (K_L) were calculated form the slope and intercept of the plot of (C_e/q_e) vs. C_e in Fig. 9(B). The parameters of the Langmiur equation were calculated and given in Table 1. The maximum adsorption capacity q_{max} for the adsorption of MB onto Fe_3O_4/NiO nano mixture mixed was found to be 40.1 mg/g. This value is higher than that of other adsorbents has been also reported with q_{max} much less than Fe_3O_4/NiO nano mixture mixed, Table 2.

Recycling

In order to investigate the reusability of Fe_3O_4/NiO as an adsorbent for MB dye, after reaction completion, the nanocomposite recovered by magnetic separation and washed with acetone and deionized water several times and drying at 60°C for 8 h. Then, the dried solid was applied for future reactions. The recycled sample were used under the same reaction conditions. The results (Fig. 10) indicated that this composite can be reused for three times and no significant change was observed in its adsorption activity.

The mechanism of preparation Fe_3O_4 and FNMMO

The sections representation of the Fe_3O_4 NPs can be seen in below reactions. Fe_3O_4 NPs with a small size particles have been synthesized by hydrolyzing an initial precursor $FeCl_3$ in a solution of EG with the addition of urea and citric acid. Citric acid is well-known for its nontoxicity, stableness and its role as a biological ligand for metal ions

Table 1. Parameters of Langmuir isotherm equations, regression coefficients (r) for the adsorption of MB on FNMMO NPs at 25 °C and pH 4.

a_L(L/mg)	K_L(L/g)	q_{max}(mg/g)	R^2
1.015	0.33	40.1	0.999

Table 2. Comparison of the maximum adsorption capacity for FNMMO NPs with various adsorbent.

Name of adsorbent	Q_{max} (mg.g^{-1})	Name of dye	Reference
Fe_3O_4-Azolla filicoloides	0.498	MB	34
Fe_3O_4@Humic acid	0.291	MB	35
Fe_3O_4@Magnetic multi wall carbon nanotube	39.8	MB	36
Zeolite-Iron oxide	4.938	MB	37
Graphene/magnetite composite	24.91	MB	38
Fe_3O_4@C	27.2	MB	39
Fe_3O_4-G@mesoporous SiO_2	28.2	MB	40
NiO/MCM-41	23.26	MB	41
NiO-EG	8.8	MB	42
NiO-Pd/C	24.47	MB	43
Kaolinite	13.99	MB	44
Pineapple leaf powder	9.28	MB	45
Husk rise	6.92	MB	46
Fe_3O_4/NiO	40.1	MB	This work

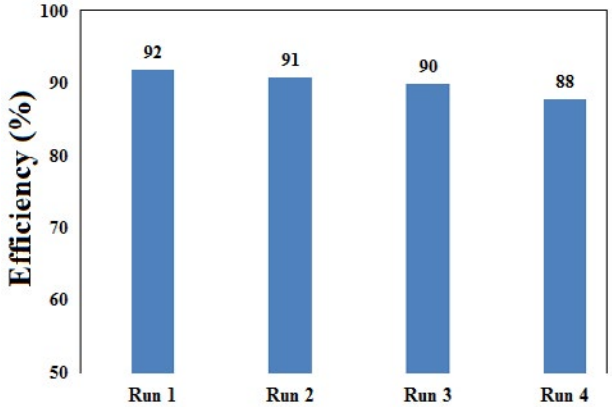

Fig. 10. The reusability of Fe_3O_4/NiO for removal of MB dye.

such as Bi^{3+}, Al^{3+}, Ca^{2+}, Fe^{3+}, Zn^{2+} and Mg^{2+} ions. Therefore, urea can be utilized as a common green organic acid for fabricating nanomaterials [47-49]. On the other hand, it has been proven that citric is a good capping agent for adjusting the relative activity of the cations and retarding the grain growth of semiconductors. The diameter of the nanoparticles can be controlled by citric acid as chelating [47,49,50].

For synthesis of Fe_3O_4 NPs, based on above discussions, speculated process for its formation can be bought out as the following. Firstly, Fe^{3+} was produced after $FeCl_3$ dissolved into the solution of EG (Eq. 1). Secondary, citric acid as an organic acid can be hydrolyzed to $[C_6O_7H_5]^{3-}$ and H^+, it has been suggested that $[C_6O_7H_5]^{3-}$ ions may chelate with $Fe3^+$ to produce $[C_6O_7H_5]^{3-}Fe^{3+}$ (Eq. 2) [49,51]. Then Fe^{3+} will be released slowly and gradually converted into $Fe(OH)_3$, since $Fe(OH)_3$ is more stable than $[C_6O_7H_5]^{3-}Fe^{3+}$ in solution. However, in the absence of citric acid, owing to no chelating effect existed and higher pH value [52], the greatly accelerated alcoholysis process of Fe^{3+} occurs rapidly (Eq. 3), resulting in the larger crystal of Fe_3O_4 particles with obvious agglomeration.

$$FeCl_3 \longrightarrow Fe^{3+} + Cl^- \quad (1)$$

$$Fe^{3+} + C_6O_7H_8 \longrightarrow [C_6O_7H_5]^{3-}Fe^{3+} + 3H^+ \quad (2)$$

$$Fe^{3+} + 3OH^- \longrightarrow Fe(OH)_3 \quad (3)$$

As we know, urea can be decomposing thermally at a relatively low temperature (below 100 °C) while releasing a high volume of gas and increasing the pH of the solution, there by promoting the precipitation of the metal as oxy/hydroxides. A further via solvothermal of these intermediates promotes their conversion into the desired metal oxides. The typical reaction of decomposition $(NH_2)_2CO$ is as follows [53]:

$$(NH_2)_2CO + 3H_2O \longrightarrow CO_2 + 2NH_4^+ + 2OH^- \quad (4)$$

We prepared Fe_3O_4 NPs using EG as a solvent with a high boiling point and the reducing agent that reduced the metal ions (Fe^{3+}) to a lower valence state (Fe^{2+}) [54]. Ethylene glycol can undergo dehydration and the so-formed acetaldehyde [55,56] reduced Fe(III) to Fe(II) and gives ferrous hydroxide in the form of a solution collide. Most likely, both ferric and ferrous oxidation states of iron coexist in the reaction mixture thus enabling magnetite formation:

$$2OH\text{-}CH_2\text{-}CH_2\text{-}OH \longleftrightarrow 2CH_3\text{-}CHO + 2H_2O \quad (5)$$

$$2CH_3\text{-}CHO + 2Fe^{3+} \longleftrightarrow CH_3\text{-}CO\text{-}CO\text{-}CH_3 + 2Fe^{2+} + 2H^+ \quad (6)$$

$$Fe^{2+} + 2OH^- \longleftrightarrow Fe(OH)_2 \quad (7)$$

$$2Fe(OH)_3 + Fe(OH)_2 \longleftrightarrow Fe_3O_4 + 4H_2O \quad (8)$$

For preparation of NiO shell, a solution of NaOH (1 M) was added in solution of Ni^{2+} to form $Ni(OH)_2$. A further calcination of these intermediates promotes their conversion into the desired metal oxide NiO. The typical reactions of preparing NiO are as follows:

$$Ni(OAc)_2 \longleftrightarrow Ni^{2+} + OAc^- \quad (11)$$

$$Ni^{2+} + 2OH^- \longleftrightarrow Ni(OH)_2 \quad (12)$$

$$Ni(OH)_2 \underset{\text{or } 500\ ^oC}{\overset{320\ ^oC}{\longleftrightarrow}} NiO + H_2O \quad (13)$$

According to various studies, such extreme chemical environments lead to the smaller sized inorganic particles. Further the ultrasonication is advantages to reducing the agglomeration of nanoparticles and the restacks of various exfoliated oxides [57,58].

Recently, Niasari et al reported an intriguing result on the size and morphology of iron vanadate nanospheres via ultrasound irradiation and various amino acids as a green capping agent [59]. More studies indicated that different factors such as sonication time, solvent and capping agents can be effect on size and other properties of prepared sampled via ultrasound irradiation [60]. Therefore, the sonochemical process significantly reduces the reaction time, achieving uniform coating of NiO nanoparticles on Fe_3O_4 core.

Furthermore, sonolysis of water generate a primary free radical species (hydrogen ($H^\bullet$) and hydroxyl ($OH^\bullet$)). The radicals can recombine to return to their original form, or recombine in like pairs, to produce molecular hydrogen (H_2) and hydrogen peroxide (H_2O_2). In oxygenated solutions, they can also produce perhydroxyl radical ($HO_2^\bullet$) by combination with O2 that finally can generate H_2O_2. These strong oxidants and reductants are utilized for various sonochemical reactions in aqueous solutions.

CONCLUSION

Based on above results and discussions, the following conclusions can be drawn in this paper:

(1) Superparamagnetic FNMMO NPs were successfully synthesized via eco-friendly method, in which raw reactants were simultaneously added into an aqueous phase, with assist of ultrasonic irradiation.

(2) The mechanism of preparation was proposed that FNMMO NPs were prepared by OH and H radicals which were got under the influence of ultrasonic process. OH^-s was dropped that were increased the rate of reactions.

(3) XRD, SEM and TEM analysis indicate that mixed methods synthesis has been completely used to prepare FNMMO NPs with diameters 60-70 nm at normal temperature and pressure via co-precipitation assisted by ultrasonic route.

(4) The Fe_3O_4/NiO nanoparticles were able to achieve 92% removal of methylene blue at pH 4. The adsorbent dose proportionally affected the color removal, and the extent of color removal decreased with increasing initial dye concentration. The maximum adsorption capacity of MB on FNMMO NPs reached 40 $mg.g^{-1}$. Thus, the present investigation provides an efficient, stable, economical and environmentally friendly adsorbent with potential for particle application in the treatment of dye water.

CONFLICT OF INTEREST

The authors declare that there are no conflicts of interest regarding the publication of this manuscript.

REFERENCES

1. Aksu Z. Application of biosorption for the removal of organic pollutants: a review. Process Biochemistry. 2005;40(3-4):997-1026.
2. Srinivasan A, Viraraghavan T. Decolorization of dye wastewaters by biosorbents: A review. Journal of Environmental Management. 2010;91(10):1915-29.
3. Crini G. Non-conventional low-cost adsorbents for dye removal: A review. Bioresource Technology. 2006;97(9):1061-85.
4. Cai X, Cai Y, Liu Y, Deng S, Wang Y, Wang Y, et al. Photocatalytic degradation properties of Ni(OH)2 nanosheets/ZnO nanorods composites for azo dyes under visible-light

irradiation. Ceramics International. 2014;40(1):57-65.
5. Hameed BH, Ahmad AA. Batch adsorption of methylene blue from aqueous solution by garlic peel, an agricultural waste biomass. Journal of Hazardous Materials. 2009;164(2-3):870-5.
6. Nasuha N, Hameed BH, Din ATM. Rejected tea as a potential low-cost adsorbent for the removal of methylene blue. Journal of Hazardous Materials. 2010;175(1-3):126-32.
7. Rafatullah M, Sulaiman O, Hashim R, Ahmad A. Adsorption of methylene blue on low-cost adsorbents: A review. Journal of Hazardous Materials. 2010;177(1-3):70-80.
8. Türgay O, Ersöz G, Atalay S, Forss J, Welander U. The treatment of azo dyes found in textile industry wastewater by anaerobic biological method and chemical oxidation. Separation and Purification Technology. 2011;79(1):26-33.
9. Ma J, Song W, Chen C, Ma W, Zhao J, Tang Y. Fenton Degradation of Organic Compounds Promoted by Dyes under Visible Irradiation. Environmental Science & Technology. 2005;39(15):5810-5.
10. Fu J, Xin Q, Wu X, Chen Z, Yan Y, Liu S, et al. Selective adsorption and separation of organic dyes from aqueous solution on polydopamine microspheres. Journal of Colloid and Interface Science. 2016;461:292-304.
11. Gawande MB, Pandey RK, Jayaram RV. Role of mixed metal oxides in catalysis science—versatile applications in organic synthesis. Catalysis Science & Technology. 2012;2(6):1113.
12. Ansari F, Salavati-Niasari M. Simple sol-gel auto-combustion synthesis and characterization of lead hexaferrite by utilizing cherry juice as a novel fuel and green capping agent. Advanced Powder Technology. 2016;27(5):2025-31.
13. Mahdiani M, Sobhani A, Ansari F, Salavati-Niasari M. Lead hexaferrite nanostructures: green amino acid sol–gel auto-combustion synthesis, characterization and considering magnetic property. Journal of Materials Science: Materials in Electronics. 2017;28(23):17627-34.
14. Miller JB, Ko EI. Control of mixed oxide textural and acidic properties by the sol-gel method. Catalysis Today. 1997;35(3):269-92.
15. Zhang J, Wang H, Dalai AK. Effects of metal content on activity and stability of Ni-Co bimetallic catalysts for CO2 reforming of CH4. Applied Catalysis A: General. 2008;339(2):121-9.
16. Gedanken A. Using sonochemistry for the fabrication of nanomaterials. Ultrasonics Sonochemistry. 2004;11(2):47-55.
17. Song G, Ma S, Tang G, Wang X. Ultrasonic-assisted synthesis of hydrophobic magnesium hydroxide nanoparticles. Colloids and Surfaces A: Physicochemical and Engineering Aspects. 2010;364(1-3):99-104.
18. Lei S, Tang K, Fang Z, Zheng H. Ultrasonic-Assisted Synthesis of Colloidal Mn3O4Nanoparticles at Normal Temperature and Pressure. Crystal Growth & Design. 2006;6(8):1757-60.
19. Ghiyasiyan-Arani M, Salavati-Niasari M, Naseh S. Enhanced photodegradation of dye in waste water using iron vanadate nanocomposite; ultrasound-assisted preparation and characterization. Ultrasonics Sonochemistry. 2017;39:494-503.
20. Maleki A, Aghaei M. Ultrasonic assisted synergetic green synthesis of polycyclic imidazo(thiazolo)pyrimidines by using Fe 3 O 4 @clay core-shell. Ultrasonics Sonochemistry. 2017;38:585-9.
21. Moreno-Valencia EI, Paredes-Carrera SP, Sánchez-Ochoa JC, Flores-Valle SO, Avendaño-Gómez JR. Diclofenac degradation by heterogeneous photocatalysis with Fe3O4/Ti x O y /activated carbon fiber composite synthesized by ultrasound irradiation. Materials Research Express. 2017;4(11):115026.
22. Li D, Zhang Y, Liu D, Yao S, Liu F, Wang B, et al. Hierarchical core/shell ZnO/NiO nanoheterojunctions synthesized by ultrasonic spray pyrolysis and their gas-sensing performance. CrystEngComm. 2016;18(41):8101-7.
23. Yudin A, Shatrova N, Khaydarov B, Kuznetsov D, Dzidziguri E, Issi J-P. Synthesis of hollow nanostructured nickel oxide microspheres by ultrasonic spray atomization. Journal of Aerosol Science. 2016;98:30-40.
24. Ramasamy Raja V, Rani Rosaline D, Suganthi A, Rajarajan M. Ultrasonic assisted synthesis with enhanced visible-light photocatalytic activity of NiO/Ag 3 VO 4 nanocomposite and its antibacterial activity. Ultrasonics Sonochemistry. 2018;44:73-85.
25. Cheng Z, Chu X, Zhong H, Yin J, Zhang Y, Xu J. Synthesis of Fe3O4 nanoflowers by a simple and novel solvothermal process. Materials Letters. 2012;76:90-2.
26. Lu W, Shen Y, Xie A, Zhang W. Green synthesis and characterization of superparamagnetic Fe3O4 nanoparticles. Journal of Magnetism and Magnetic Materials. 2010;322(13):1828-33.
27. Kalska-Szostko B, Wykowska U, Satuła D. Magnetic nanoparticles of core–shell structure. Colloids and Surfaces A: Physicochemical and Engineering Aspects. 2015;481:527-36.
28. Ben Youssef J, Layadi A. Ferromagnetic resonance study of Permalloy/Cu/Co/NiO spin valve system. Journal of Applied Physics. 2010;108(5):053913.
29. Mendez-Garza J, Wang B, Madeira A, Giorgio CD, Bossis G. Synthesis and Surface Modification of Spindle-Type Magnetic Nanoparticles: Gold Coating and PEG Functionalization. Journal of Biomaterials and Nanobiotechnology. 2013;04(03):222-8.
30. Fu, M., Xie, Y. & Zhong, X. One-Step Magnet-Induced Solvent Thermal Synthesis of. *Ijrras* 15, 154–157 (2013).
31. Peng D, Beysen S, Li Q, Jian J, Sun Y, Jiwuer J. Hydrothermal growth of octahedral Fe3O4 crystals. Particuology. 2009;7(1):35-8.
32. Bhaumik M, Leswifi TY, Maity A, Srinivasu VV, Onyango MS. Removal of fluoride from aqueous solution by polypyrrole/Fe3O4 magnetic nanocomposite. Journal of Hazardous Materials. 2011;186(1):150-9.
33. Gupta VK, Agarwal S, Saleh TA. Chromium removal by combining the magnetic properties of iron oxide with adsorption properties of carbon nanotubes. Water Research. 2011;45(6):2207-12.
34. Rakhshaee R, Giahi M, Pourahmad A. Removal of methyl orange from aqueous solution by Azolla filicoloides: Synthesis of Fe3O4 nano-particles and its surface modification by the extracted pectin of Azolla. Chinese Chemical Letters. 2011;22(4):501-4.
35. Zhang X, Zhang P, Wu Z, Zhang L, Zeng G, Zhou C. Adsorption of methylene blue onto humic acid-coated Fe3O4 nanoparticles. Colloids and Surfaces A: Physicochemical and Engineering Aspects. 2013;435:85-90.
36. Gong J-L, Wang B, Zeng G-M, Yang C-P, Niu C-G, Niu Q-Y, et al. Removal of cationic dyes from aqueous solution using magnetic multi-wall carbon nanotube nanocomposite as adsorbent. Journal of Hazardous Materials. 2009;164(2-

3):1517-22.
37. Dwivedi, M. K., Rashmi Agrawal, and Pragati Sharma. "Adsorptive Removal of Methylene Blue from Wastewater Using Zeolite-Iron Oxide Magnetic Nanocomposite." *International Journal of Advanced Research in Science and Engineering*5.2 (2016): 515-522.
38. Ai L, Zhang C, Chen Z. Removal of methylene blue from aqueous solution by a solvothermal-synthesized graphene/ magnetite composite. Journal of Hazardous Materials. 2011;192(3):1515-24.
39. Zhang Z, Kong J. Novel magnetic Fe3O4@C nanoparticles as adsorbents for removal of organic dyes from aqueous solution. Journal of Hazardous Materials. 2011;193:325-9.
40. Wu X-L, Shi Y, Zhong S, Lin H, Chen J-R. Facile synthesis of Fe3O4-graphene@mesoporous SiO2 nanocomposites for efficient removal of Methylene Blue. Applied Surface Science. 2016;378:80-6.
41. Xiao X, Zhang F, Feng Z, Deng S, Wang Y. Adsorptive removal and kinetics of methylene blue from aqueous solution using NiO/MCM-41 composite. Physica E: Low-dimensional Systems and Nanostructures. 2015;65:4-12.
42. Zhu T, Chen JS, Lou XW. Highly Efficient Removal of Organic Dyes from Waste Water Using Hierarchical NiO Spheres with High Surface Area. The Journal of Physical Chemistry C. 2012;116(12):6873-8.
43. Arabzadeh, S., et al. "Comparison of nickel oxide and palladium nanoparticle loaded on activated carbon for efficient removal of methylene blue: Kinetic and isotherm studies of removal process." *Human & experimental toxicology* 34.2 (2015): 153-169.
44. Ayad MM, El-Nasr AA. Adsorption of Cationic Dye (Methylene Blue) from Water Using Polyaniline Nanotubes Base. The Journal of Physical Chemistry C. 2010;114(34):14377-83.
45. Weng C-H, Lin Y-T, Tzeng T-W. Removal of methylene blue from aqueous solution by adsorption onto pineapple leaf powder. Journal of Hazardous Materials. 2009;170(1):417-24.
46. Vadivelan V, Kumar KV. Equilibrium, kinetics, mechanism, and process design for the sorption of methylene blue onto rice husk. Journal of Colloid and Interface Science. 2005;286(1):90-100.
47. Liu X, Guo Y, Wang Y, Ren J, Wang Y, Guo Y, et al. Direct synthesis of mesoporous Fe3O4 through citric acid-assisted solid thermal decomposition. Journal of Materials Science. 2010;45(4):906-10.
48. Zhang K, Liang J, Wang S, Liu J, Ren K, Zheng X, et al. BiOCl Sub-Microcrystals Induced by Citric Acid and Their High Photocatalytic Activities. Crystal Growth & Design. 2012;12(2):793-803.
49. Huo Y, Jin Y, Zhang Y. Citric acid assisted solvothermal synthesis of BiFeO3 microspheres with high visible-light photocatalytic activity. Journal of Molecular Catalysis A: Chemical. 2010;331(1-2):15-20.
50. Mou Y, Yang H, Xu Z. Morphology, Surface Layer Evolution, and Structure–Dye Adsorption Relationship of Porous Fe3O4 MNPs Prepared by Solvothermal/Gas Generation Process. ACS Sustainable Chemistry & Engineering. 2017;5(3):2339-49.
51. Field TB, McCourt JL, McBryde WAE. Composition and Stability of Iron and Copper Citrate Complexes in Aqueous Solution. Canadian Journal of Chemistry. 1974;52(17):3119-24.
52. Popa M, Preda S, Fruth V, Sedlácková K, Balázsi C, Crespo D, et al. BiFeO3 films on steel substrate by the citrate method. Thin Solid Films. 2009;517(8):2581-5.
53. Jiang W, Cao Z, Gu R, Ye X, Jiang C, Gong X. A simple route to synthesize ZnFe2O4hollow spheres and their magnetorheological characteristics. Smart Materials and Structures. 2009;18(12):125013.
54. Cha J, Lee JS, Yoon SJ, Kim YK, Lee J-K. Solid-state phase transformation mechanism for formation of magnetic multi-granule nanoclusters. RSC Advances. 2013;3(11):3631.
55. Smith WB. Ethylene glycol to acetaldehyde-dehydration or a concerted mechanism. Tetrahedron. 2002;58(11):2091-4.
56. Skrabalak SE, Wiley BJ, Kim M, Formo EV, Xia Y. On the Polyol Synthesis of Silver Nanostructures: Glycolaldehyde as a Reducing Agent. Nano Letters. 2008;8(7):2077-81.
57. Kozakova Z, Kuritka I, Kazantseva NE, Babayan V, Pastorek M, Machovsky M, et al. The formation mechanism of iron oxide nanoparticles within the microwave-assisted solvothermal synthesis and its correlation with the structural and magnetic properties. Dalton Trans. 2015;44(48):21099-108.
58. Suslick KS, Price GJ. APPLICATIONS OF ULTRASOUND TO MATERIALS CHEMISTRY. Annual Review of Materials Science. 1999;29(1):295-326.
59. Ghiyasiyan-Arani M, Salavati-Niasari M, Masjedi-Arani M, Mazloom F. An easy sonochemical route for synthesis, characterization and photocatalytic performance of nanosized FeVO4 in the presence of aminoacids as green capping agents. Journal of Materials Science: Materials in Electronics. 2017;29(1):474-85.
60. Monsef R, Ghiyasiyan-Arani M, Salavati-Niasari M. Application of ultrasound-aided method for the synthesis of NdVO4 nano-photocatalyst and investigation of eliminate dye in contaminant water. Ultrasonics Sonochemistry. 2018;42:201-11.
61. Weissler A. Formation of Hydrogen Peroxide by Ultrasonic Waves: Free Radicals. Journal of the American Chemical Society. 1959;81(5):1077-81.